A method to recover water-wave profiles from pressure measurements

Vishal Vasan[a,*], Katie Oliveras[b], Diane Henderson[a], Bernard Deconinck[c]

[a] *Department of Mathematics, Pennsylvania State University, University Park, PA 16802*
[b] *Department of Mathematics, Seattle University, Seattle, WA 98122*
[c] *Department of Applied Mathematics, University of Washington, Seattle, WA 98195*

Abstract

An operational formulation is proposed for reconstructing a time series of water surface displacement from waves using measurements from a pressure transducer located at an arbitrary depth. The approach is based on the fully nonlinear formulation for pressure below traveling-wave solutions of Euler's equations developed in [1]. Its validity is tested using experiments in which both the pressure and the surface displacement are measured. The experiments include a wave system that is Galilean invariant – cnoidal waves, and wave systems that are not – reflected cnoidal waves and wave groups. We find that since the proposed formulation is nonlinear, it reproduces the amplitude spectrum of the measured surface displacements better than the hydrostatic model and better than the linear model that takes into account the pressure response factor due to small amplitude waves (the transfer function). Both the proposed formula and the transfer function reconstruct the surface reasonably well, with the proposed formula being about 5% more accurate.

Keywords: water waves, pressure, recovery, measurement

1. Introduction

Pressure transducers are a common device for measuring surface water waves in both the laboratory and the field. However, the inversion from time series of pressure to time series of surface displacement is nontrivial. The relationship between pressure and surface displacement, based on the Stokes boundary value problem [2], is nonlinear and involves water particle velocities. In

*Corresponding author at: Department of Mathematics, Pennsylvania State University, University Park, PA 16802
Email address: vxv10@psu.edu (Vishal Vasan)

practice, various approximate relationships are used. A common [3] relation between the surface displacement spectrum S_f and the pressure spectrum S_p is

$$S_f = NS_p/K_p, \tag{1}$$

where N is an empirical factor, and

$$K_p = \frac{\cosh k(h+z)}{\cosh kh} \tag{2}$$

is the pressure response factor, which is obtained from linear theory and takes into account pressure due to wave motion. Here, h is the water depth; k is the radian wavenumber related to radian wave frequency ω through the linear dispersion relation $\omega^2 = gk\tanh(kh)$; g is the acceleration of gravity and $z < 0$ is the vertical depth of the pressure transducer, measured positive upward from the still water level. The empirical factor $N = 1$ corresponds to linear wave theory. The conventional wisdom from the Shore Protection Manual [3] is that N decreases with decreasing period; $N > 1$ for long-period waves, and $N < 1$ for short-period waves.

There have been many field and laboratory studies to determine if linear theory provides an adequate relationship between pressure measurements and surface displacement, and some disagreement exists. Bishop & Donelan [4] reviewed these studies. They concluded that linear wave theory is adequate for obtaining surface wave heights from pressure gage data to within 5%, except when measuring waves in shallow water. For waves in shallow water, they concurred with [5] that one must use $N \neq 1$ in order to account for currents and wave nonlinearity. Also energy from higher frequency waves is not recovered adequately by (1) because the higher frequency velocities fall off rapidly with increasing depth, because of inherent limitations of the pressure transducers and because of spectral leakage to high frequencies due to the form of K_p.

Typically, nonlinear effects are included using a Stokes expansion to obtain higher order corrections. There have been studies using Stokes expansions to 2nd order [5], to 3rd order, and 5th order [6]. Tsai *et. al* [7] reviewed these results, some of which showed improvement over linear theory and some of which did not. They concluded both that "These seemingly incoherent results in fact only reflect the different wave conditions being studied." and that "... it is universally understood that the non linear correction is essential in shallow water or in surf zone." Alternative approaches have been considered. For example, Chen [8] used a higher order expansion to find an

empirical nonlinear transfer function with a frequency parameter and a depth of gage submergence parameter. Kuo & Chiu [9] used dimensional analysis to develop an empirical formula from data, which Baquerizo & Losada [10] showed could be obtained from the pressure response factor (with a reply in [11]). Fully nonlinear models for surface displacement recovery based on the equations for traveling water waves were presented in [1, 12–15]. A neural network approach is given in [16] and [17].

The subject remains an area of importance and on-going work. Indeed, the array of about 40 DART (Deep-ocean Assessment and Reporting of Tsunamis) buoys used for obtaining real-time surface-displacement data for tsunami forecasting rely on pressure measurements, as do measurements of storm surge from hurricanes [18].

In this paper, we address the need for obtaining a nonlinear mapping from pressure to surface displacement following Oliveras *et al* [1]. Rather than starting with the Stokes boundary value problem and proceeding with a perturbation expansion in the surface displacement and velocity potential, we started with a reformulation of the Stokes boundary value problem given by [19]. From this representation, we found an exact formulation for the surface displacement that requires the numerical solution of a nonlocal, nonlinear equation. The errors with respect to nonlinearity do not exceed machine precision. In this formulation, we make two assumptions: (i) that the pressure transducers are situated at the bottom of the fluid domain, and (ii) that surface displacements are due to a traveling wave system. This theory is reviewed in §2. Many of the papers discussed above, such as [8] have shown that transducer depth is important. Therefore in §3 we expand the result in [1] to allow for an arbitrary depth of the pressure transducer. Currents are important as well. Thus in Appendix A we discuss an extension to the theory that allows for a constant vorticity following Vasan & Oliveras [20]. A summary of the theoretical results presented is:

- The general formula from [1] has no approximation on type of nonlinearity; however solutions must be found numerically, albeit to machine precision.
- To obtain an explicit, operational formulation, we truncate the order of nonlinearity and propose a formula to replace (1) in practice. (The fully nonlinear formulation from [1] makes asymptotics quite straightforward.)
- The proposed formulation assumes a traveling wave system, and so requires a wave speed, which is assumed to be the same for all frequency components.

  - The standard, linear inversion, (1) with the empirical constant $N = 1$, is a special case of the formulation presented here, thus, the assumption of traveling waves does not limit the associated generality of the present results more than (1) does.
  - Since measurements comprise time series at fixed locations, some value of the wave speed is required by all models to map from time data to spatial data.
  - Oliveras & Vasan [21] reformulated the mapping so that the value of the speed is not required. We do not use their results herein, as discussed in §3.

- The formulation presented here allows the pressure transducer to be at any depth in the water column.

- The new formulation allows for constant vorticity, which introduces new phenomena.

In [1] we developed various approximations to their fully nonlinear pressure-to-surface displacement mapping. We compared the fully nonlinear mapping and these approximations with numerical solutions and with experimental measurements of solitary waves that used both surface capacitance gages and bottom, pressure transducers. Here we report also on experimental comparisons with predictions to see if the proposed formula works for wave systems that break the assumption of a traveling wave system. The experimental apparatus is presented in §4. Results are presented in §5 for experiments that use cnoidal waves, which give a periodic, traveling wave system as assumed by the theory, and for experiments that use reflecting cnoidal waves and wave groups, neither of which comprise traveling wave systems. We summarize results in §6.

Our main conclusion is that since the proposed formula is nonlinear, it reproduces the amplitude spectrum of the measured surface displacements better than does the transfer function (1) with the empirical constant $N = 1$. The experiments show that both the proposed formula and the transfer function reconstruct the surface displacement reasonably well, with predictions from the proposed formula being about 5% more accurate. Hence, we claim that the proposed formula presented here provides a better mapping from time series measurements of pressure to time series of surface displacement than is otherwise available. It is more accurate than (1), requires just one more Fourier transform, is no less general because of the assumption of traveling waves, and it can include an arbitrary depth for the pressure transducer.

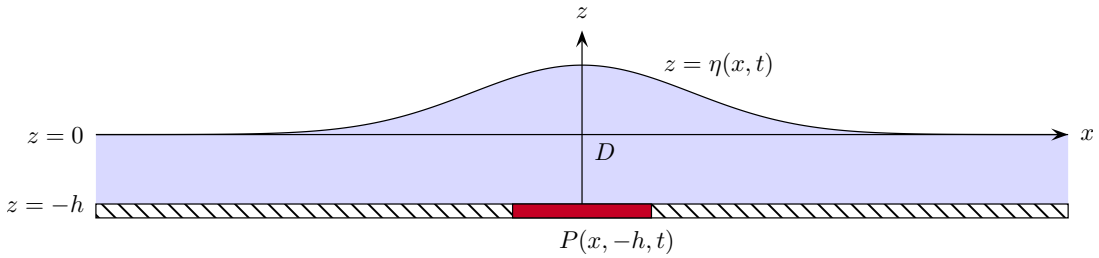

Figure 1: The fluid domain D for the water wave problem. A pressure sensor is indicated at the bottom. In our calculations the pressure measurement is assumed to be a point measurement.

2. Theory

Consider Euler's equations describing the dynamics of the surface of an ideal irrotational fluid in two dimensions (with a one-dimensional surface):

$$\phi_{xx} + \phi_{zz} = 0, \qquad (x, z) \in D, \tag{3}$$

$$\phi_z = 0, \qquad z = -h, \tag{4}$$

$$\eta_t + \eta_x \phi_x = \phi_z, \qquad z = \eta(x, t), \tag{5}$$

$$\phi_t + \frac{1}{2}\left(\phi_x^2 + \phi_z^2\right) + g\eta = 0, \qquad z = \eta(x, t), \tag{6}$$

where $\phi(x, z, t)$ represents the velocity potential of the fluid with surface elevation $\eta(x, t)$. A solution to the above set of equations consists of finding a potential ϕ that satisfies Laplace's equation inside the fluid domain D, sketched in Figure 1, as well as finding the graph of the free surface η. Below we pose the problem on the whole line $x \in \mathbb{R}$, assuming the velocities (and surface profile) decay at infinity. The problem may also be posed using periodic boundary conditions. The only change in the resulting relations being that the Fourier series is employed in the place of the Fourier transform.

Our goal is to relate the pressure measured at a sensor $P(x_0, -h, t)$, which is also sketched in Figure 1, located on the bottom boundary of the fluid, to the surface elevation profile $\eta(x_0, t)$. As stated, equations (3-6) do not involve the pressure field. However, we note that the following Bernoulli condition valid in the interior of the fluid:

$$\phi_t + \frac{1}{2}\left(\phi_x^2 + \phi_z^2\right) + gz + \frac{P(x, z, t)}{\rho} = 0, \quad -h \le z \le \eta(x, t). \tag{7}$$

The overall scheme is as follows. Since (7) is valid at the bottom boundary, we employ this relation to convert the pressure measurement into a condition on the velocity potential at $z = -h$. In addition, we note from equations (5-6), that the velocity potential at the surface is related to the surface elevation profile. Since the potential ϕ satisfies Laplace's equation, the boundary values of the potential at $z = -h$ and $z = \eta$ must be related. This consistency of boundary values forms the basis of our reconstruction method.

The scheme described in the previous paragraph involves connecting boundary data at the bottom and top surfaces. Setting $\phi_z(x, -h, t) = 0$ in equation (7) we obtain a relation between the bottom pressure $P(x, -h, t)$ and $\phi(x, -h, t)$. A major difficulty in the problem of surface reconstruction, however, is that the input data is typically a time series of the pressure at $z = -h$ for a single spatial point (or discrete set of points), *i.e.*, $P_j(x_j, -h, t)$, $j = 1, 2, \ldots$, where x_j need not be spaced close together. In our experiments, as well as in field experiments, we typically deal with only one spatial location x_0. Therefore, we require a method to convert $P(x_0, -h, t)$ to $P(x, -h, t)$. Further, having recovered $P(x, -h, t)$, we seek $\phi(x, -h, t)$ through (7). We claim this is not practical without further simplification. To see why, consider (7) as a partial differential equation for $\phi(x, -h, t)$ with $P(x, -h, t)$ as a forcing term. Evidently we require knowledge of an initial state for $\phi(x, -h, t)$, *i.e.*, an initial condition.

In the following, we restrict to the case of a traveling wave moving with velocity c. This assumption permits us to translate time series data to spatial information, establishes the initial state of the fluid (indeed the state for all time) and permits the study of nonlinear effects. One of the primary aims of the current work is to understand how nonlinear effects may be incorporated to increase the accuracy of surface reconstruction. Of course, assuming a traveling wave comes at a cost. The speed of the wave is required to translate the time series data to a spatial measurement.

A pictographic overview of the reconstruction method is shown in Figure 2. Although not explictly indicated in the figure, the wave speed does appear in the reconstruction of $\eta(x, t_0)$ from $P(x, -h, t_0)$, *i.e.*, the central part of Figure 2. In [22] the authors investigated the dependence on the speed c for this part of the reconstruction algorithm for numerically computed traveling water wave solutions to Euler's equations. They found that the method introduced in [1] was particularly insensitive to errors in the wave speed. In the present work we investigate the effect of the speed of the wave particularly for the conversion from time series to spatial data for pressure measurements from physical experiments. For the conversion from $P(x, -h, t_0) \to \eta(x, t_0)$, in the current work, we

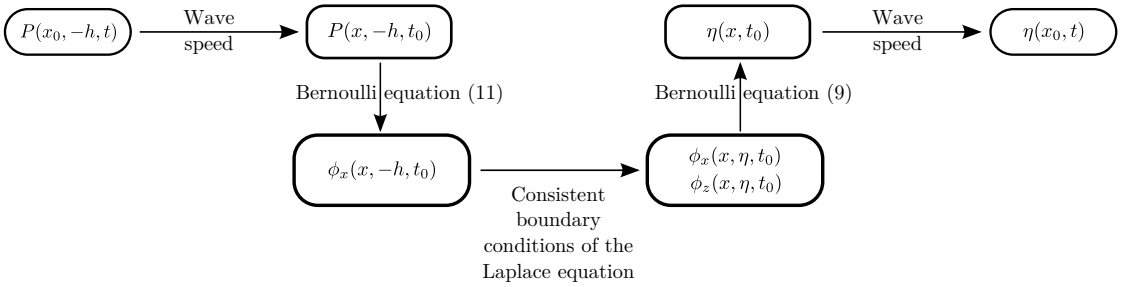

Figure 2: Summary of the surface reconstruction algorithm.

employ three speed-independent asymptotic reductions obtained from the fully nonlinear method of [1]. They are the hydrostatic model, the transfer function (1) with the empirical constant $N = 1$, and the proposed formula (23).

Remark 1. *In §5 we present the reconstruction of the water wave surface for two interacting traveling waves and a wave group. These experiments imply different choices for the wave speed to convert the time series data into a spatial measurement. This is, in part, why we do not use the traveling wave variable $x - ct$ in Figure 2.*

Now we present a review of the derivation for the fully nonlinear reconstruction algorithm from $P(x, -h, t_0) \to \eta(x, t_0)$ under the assumption of a traveling wave [1]. Our goal is to obtain from this the asymptotic reconstruction formulae. We introduce $\xi = x - ct$ and assume all dynamical quantities depend only on ξ, so that x and t-derivatives become ξ-derivatives, the latter multiplied by $-c$. The Bernoulli and kinematic boundary conditions at the free surface $z = \eta$ become:

$$-c\eta_\xi + \eta_\xi \Phi_\xi = \Phi_z, \qquad z = \eta(\xi), \tag{8}$$

$$-c\Phi_\xi + \frac{1}{2}\left(\Phi_\xi^2 + \Phi_z^2\right) + g\eta = 0, \qquad z = \eta(\xi), \tag{9}$$

where $\Phi(\xi, z) = \phi(x, z, t)$. Equations (8-9) are an algebraic set of relations for the velocities at the surface from which we obtain

$$\Phi_\xi(\xi, \eta) = c - \sqrt{\frac{c^2 - 2g\eta}{1 + \eta_\xi^2}}, \tag{10a}$$

$$\Phi_z(\xi, \eta) = -\eta_\xi \sqrt{\frac{c^2 - 2g\eta}{1 + \eta_\xi^2}}, \tag{10b}$$

where for $c > 0$ we choose the $-$ sign, to ensure that the local horizontal velocity is less than the wave speed [23]. Similarly, for $c < 0$ the $+$ sign should be chosen. In the following we choose $c > 0$, restricting to rightward traveling waves. This simple calculation allows us to express the gradient of the velocity potential at the surface directly in terms of the surface elevation.

A similar consideration for the Bernoulli condition (7) at the bottom boundary $z = -h$ leads to

$$-cQ_\xi + \frac{1}{2}Q_\xi^2 - gh + \frac{P(\xi, -h)}{\rho} = 0, \tag{11}$$

where $Q(\xi) = \Phi(\xi, -h)$ is the velocity potential at the bottom of the fluid, and we have changed to the traveling coordinate frame as before. Then (11) is a quadratic equation for Q_ξ from which we find

$$Q_\xi = c - \sqrt{c^2 - 2p}, \tag{12}$$

where $p(\xi)$ is the non-static part of the pressure at the bottom in the traveling coordinate frame, scaled by the fluid density: $p(\xi) = -gh + P(\xi, -h)/\rho$. As before we choose the $-$ sign to be consistent with rightward traveling waves.

Within the bulk of the fluid D,

$$\Phi_{\xi\xi} + \Phi_{zz} = 0, \tag{13}$$

where the boundary conditions given in (10a, 10b) and (12) must also be satisfied. A potential consistent with irrotational gravity waves must satisfy the associated kinematic conditions (4) and (5). Thus we let

$$\Phi(\xi, z) = \frac{1}{2\pi}\int_{-\infty}^{\infty} e^{ik\xi}\Psi(k)\cosh\left(k\left(z + h\right)\right)\, dk, \tag{14}$$

so that equation (4) is automatically satisfied. Here, we have assumed that the fluid velocities decay at infinity in the horizontal direction. Using the boundary condition at the bottom for Φ_ξ we find

$$\frac{1}{2\pi}\int_{-\infty}^{\infty} ike^{ik\xi}\Psi(k)\, dk = c - \sqrt{c^2 - 2p}, \tag{15}$$

so that

$$ik\Psi(k) = 2\pi c\delta(k) - \mathcal{F}\left\{\sqrt{c^2 - 2p}\right\}(k), \tag{16}$$

where $\delta(k)$ is the Dirac delta function and $\mathcal{F}$ denotes the Fourier transform: $\mathcal{F}\{y(\xi)\}(k) =$

$\int_{-\infty}^{\infty} y(\xi)\exp(-ik\xi)d\xi$. The form (14) implies $\Phi_\xi(\xi,z)$ at the surface $z=\eta$, which is given by

$$\Phi_\xi(\xi,\eta) = \frac{1}{2\pi}\int_{-\infty}^{\infty} e^{ik\xi} ik\Psi(k)\cosh\left(k\left(\eta+h\right)\right)\,dk \tag{17}$$

$$= c - \frac{1}{2\pi}\int_{-\infty}^{\infty} e^{ik\xi}\cosh\left(k\left(\eta+h\right)\right)\mathcal{F}\left\{\sqrt{c^2-2p}\right\}(k)\,dk. \tag{18}$$

Using (18) and the boundary condition (10a), the consistency of boundary conditions leads to the nonlocal, fully nonlinear relationship

$$\sqrt{\frac{c^2-2g\eta}{1+\eta_\xi^2}} = \frac{1}{2\pi}\int_{-\infty}^{\infty} e^{ik\xi}\cosh\left(k\left(\eta+h\right)\right)\mathcal{F}\left\{\sqrt{c^2-2p}\right\}(k)\,dk. \tag{19}$$

The above relation is a nonlinear equation for η given p and c. A rigorous justification of the above relation is presented in [1]. The analogous relationship for periodic boundary conditions is given by replacing integrals with the appropriate summation.

One advantage of a fully nonlinear model such as (19), is the ease with which various approximate models, valid in different physical regimes, may be derived. Let ϵ,μ represent the amplitude and shallowness parameters, *i.e.*, $\epsilon = a/h$ and $\mu = h/L$, where a is the wave amplitude and L is the characteristic horizontal length scale (say, the wavelength). We define the following non-dimensional variables

$$\tilde{\xi} = \xi/L, \quad \tilde{z} = z/h, \quad \tilde{\eta} = \eta/a, \quad \tilde{k} = Lk, \quad \tilde{c} = c/\sqrt{gh}, \quad \tilde{p} = p/ga.$$

Equation (19) in non-dimensional variables is given by

$$\sqrt{\frac{\tilde{c}^2-2\epsilon\tilde{\eta}}{1+\epsilon^2\mu^2\tilde{\eta}_{\tilde{\xi}}^2}} = \frac{1}{2\pi}\int_{-\infty}^{\infty} e^{i\tilde{k}\tilde{\xi}}\cosh\left(\mu\tilde{k}\left(\epsilon\tilde{\eta}+1\right)\right)\mathcal{F}\left\{\sqrt{\tilde{c}^2-2\epsilon\tilde{p}}\right\}(\tilde{k})\,d\tilde{k}. \tag{20}$$

One may Taylor expand in ϵ and/or μ to any required order and obtain asymptotically-equivalent reduced reconstruction models. In [1], we obtain and compare several models with numerical results and laboratory experiments on solitons. Here, we quote three of these models in their dimensional forms and compare their reconstuctions of measured time series of pressure in §5. Two of these are standard models discussed in §1: the hydrostatic approximation

$$\eta = \frac{p}{g}, \tag{21}$$

and the transfer function (1) with the empirical constant $N=1$, which gives a linear, dynamic correction to the hydrostatic approximation;

$$\mathcal{F}[\eta] = \cosh(kh)\mathcal{F}\left[\frac{p}{g}\right]. \tag{22}$$

The third is the proposed model

$$\eta = \frac{\mathcal{F}^{-1}\left[\cosh(kh)\mathcal{F}\left[\frac{p}{g}\right]\right]}{1-\mathcal{F}^{-1}\left[k\sinh(kh)\mathcal{F}\left[\frac{p}{g}\right]\right]}, \tag{23}$$

which yields the best results of all of the reduced models in the comparisons reported in [1]. We call (23) the "heuristic model". Aside from being common reconstruction methods employed in practice (in the case of the hydrostatic and transfer function), our study of surface displacement recovery is limited to these models as none of them have an explicit dependence on the wave-speed c.

Each of the above models for surface reconstruction can be obtained through an asymptotic expansion of (19). The hydrostatic model (21) is obtained to lowest order in the shallow water regime (retaining only $\mathcal{O}(1)$ terms or in other words setting $\epsilon = \mu = 0$), whereas the transfer function (22) is obtained by linearizing the fluid equations, *i.e.*, by expanding (20) in ϵ and retaining all terms up to $\mathcal{O}(\epsilon)$. The heuristic model (23) can be thought of as a nonlinear correction to the transfer function. Indeed this model is obtained by including particular terms of a small amplitude expansion of (19); see [1] for details. We note that each of the above asymptotic models are independent of the wave speed c. However, higher order models, in μ or ϵ, typically involve the wave speed.

We note that the traditional approach to obtaining the transfer function is by linearizing the equations for surface gravity waves. However, here we obtain the same result by linearizing (19) which is a consequence of assuming a traveling water wave. Thus, (22) can be formally interpreted for either traveling waves or small-amplitude linear waves. Consequently, we employ this model to reconstruct small-amplitude surface gravity waves with no specific speed. Similarly we may reinterpret (23) in the context of small-amplitude time-dependent wave motion. Indeed, the above analysis suggests suitable nonlinear corrections to (22) which we claim are relevant to generic time-dependent shallow water-wave surface profile reconstruction based on our experiments.

In practice, the difference between assuming a traveling wave with speed c and small-amplitude water waves amounts to choosing a wave speed to convert the time series data $P(x_0, -h, t)$ to the spatial measurement $P(x, -h, t_0)$. Mathematically this implies a relationship between the wave number k and the frequency ω, *i.e.*, $\omega = ck$ for nonlinear traveling waves and

$$\omega = \sqrt{gk\tanh(kh)}, \tag{24}$$

for small amplitude waves. Here we have chosen only one branch of the dispersion relation since, to be consistent with the fully nonlinear model, we restrict ourselves to waves traveling in one direction alone. Note that each of the above relations may be solved for k as a function of ω. Consequently, we observe that the reconstruction models (22) and (23) depend *implicitly* on the wave speed. See Section 4.1 for details on the inversion of the dispersion relation (24).

3. Pressure transducer at arbitrary depth

In the following we extend the algorithm of [1] to allow reconstruction of the surface profile from pressure measurements at an arbitrary height below the free surface. For an extension of the algorithm that accounts for a constant shear, *i.e.*, constant vorticity, see Appendix A. In either case we assume a traveling water wave with speed c.

In §2 we assumed the pressure was measured at the bottom boundary. This requirement is not essential. Here we adapt the method for surface profile reconstruction to the case when the pressure data is recorded at some height between the free surface and bottom boundary. We restrict ourselves to a case where the measuring station does not have a significant impact on the fluid flow, so that the pressure signal P_0 is at a constant height $z = -z_0$ ($-h < -z_0 < \min \eta$). Since the potential $\Phi(\xi, z)$ satisfies Laplace's equation in the domain $-h < z < -z_0$, we employ a similar technique of consistent boundary conditions to map the given non-static pressure data, $p_0 = P(\xi, -z_0)/\rho - gz_0$, to the corresponding pressure signal at the bottom boundary $p(\xi, -h)$ and thus the results from the previous section become available.

Consider a harmonic function

$$\Phi_{\xi\xi} + \Phi_{zz} = 0, \qquad -h < z < -z_0,$$

such that $\Phi_z(\xi, -h) = 0$ and $\Phi_\xi(\xi, -z_0)$ is prescribed. Assuming the gradient of Φ decays for large $|\xi|$ (alternatively, the gradient is periodic in ξ), this boundary-value problem has a well-defined solution. In particular we obtain the following relation between the Fourier transforms, using (14), of the components of $\nabla\Phi$ evaluated at $z = -z_0$:

$$\mathcal{F}[\Phi_z(\xi, -z_0)] = -i \tanh(k(h - z_0))\mathcal{F}[\Phi_\xi(\xi, -z_0)] = 0. \tag{25}$$

However, $\nabla\Phi$ is assumed to correspond to the velocity of an inviscid irrotational traveling water

wave with speed c. Hence

$$-c\Phi_\xi + \frac{1}{2}\Phi_\xi^2 + \frac{1}{2}\Phi_z^2 + p_0 = 0, \quad z = -z_0, \tag{26}$$

as a consequence of the Bernoulli condition in the bulk of the fluid. Solving (26) for Φ_ξ and substituting in (25), we have

$$\mathcal{F}[\Phi_z(\xi, -z_0)] = -i\tanh(k(h - z_0))\mathcal{F}\left[c - \sqrt{c^2 - 2p_0 - [\Phi_z(\xi, -z_0)]^2}\right]. \tag{27}$$

Thus, given a pressure signal at some height $-z_0$, we solve (27) for the vertical velocity at $z = -z_0$. In numerical tests, a simple iterative scheme based on (27) was sufficient to converge to the true value. Once $\Phi_z(\xi, -z_0)$ is computed we consider the boundary-value problem

$$\Phi_{\xi\xi} + \Phi_{zz} = 0, \qquad -h < z < -z_0, \tag{28a}$$

$$\Phi_z = 0, \qquad z = -h, \tag{28b}$$

$$\Phi_z = f(\xi), \qquad z = -z_0, \tag{28c}$$

where $f(\xi)$ is the solution of (27) for a given p_0. The horizontal boundary conditions are assumed to be either periodic or vanishing at infinity. The solution to (28a-28c) leads to an expression for $\Phi_\xi(\xi, -h)$. Again we assume the potential is consistent with a traveling water wave, so the velocity component $\Phi_\xi(\xi, -h)$ obtained must satisfy the Bernoulli condition at $z = -h$, (11). Hence, we obtain the following relation

$$\mathcal{F}\left[c - \sqrt{c^2 - 2p}\right] = \operatorname{sech}(k(h - z_0))\mathcal{F}\left[c - \sqrt{c^2 - 2p_0 - [\Phi_z(\xi, -z_0)]^2}\right], \tag{29}$$

where p is the non-static component of the pressure at the bottom boundary $z = -h$, and we have used (12) to replace $\Phi_\xi(\xi, -h)$. Equations (27) and (29) form the basis for surface elevation reconstruction from pressure measurements taken in the bulk of the fluid. Once the bottom pressure p is obtained from these equations we may use (19), or indeed (21-23), to obtain the free surface profile.

Remark 2. *In order to obtain the pressure $p(\xi)$ at $z = -h$ from (27) and (29), we assume the wave-speed c is known. However, as in the derivation of the reduced models (21-23), in an asymptotic sense, we can recover $p(\xi)$ from $p_0(\xi)$ without the wave-speed. Indeed, in the appropriate scaling, we observe from (27) that $\Phi_z(\xi, -z_0)$ is of the same order as $p_0(\xi)$. Hence, from (29) we see that*

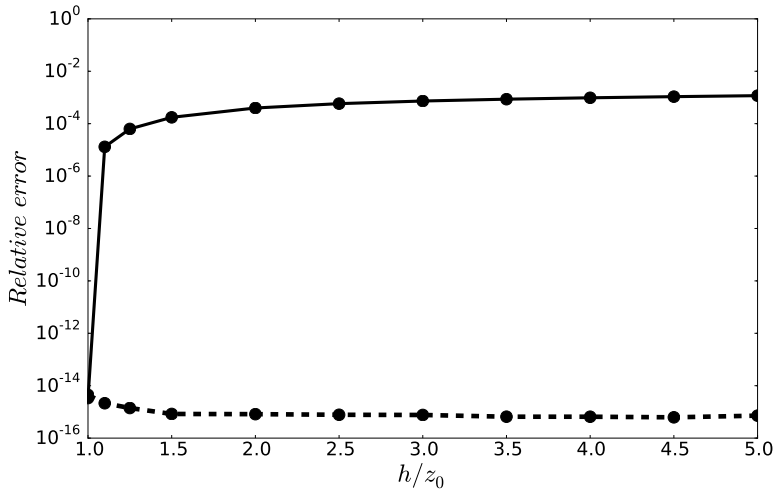

Figure 3: Relative error in the bottom pressure $p(\xi, -h)$ recovered from pressure $p_0(\xi, -z_0)$, measured at $z = -z_0$ as a function of h/z_0 beneath numerically computed periodic traveling wave solutions to Euler's equations. The dashed line represents $p(\xi, -h)$ recovered from (27) and (29), *i.e.*, when the wave speed c is known, whereas the solid line depicts bottom pressure recovery using the asymptotic relationship (30). In either case, we compute the true bottom pressure using the method described in [20]. We obtain periodic traveling wave solutions using the method of Deconinck & Oliveras [24].

to lowest order

$$\mathcal{F}[p] = \operatorname{sech}(k(h - z_0))\mathcal{F}[p_0]\,. \tag{30}$$

Thus, to reconstruct the surface displacement when the pressure transducer is at $z = -z_0$, one uses (30) to obtain $\mathcal{F}[p]$ evaluated at $z = -h$, followed by (23) to obtain η. Figure 3 shows the relative errors obtained from using the full formulation from (27) and (29) versus those obtained from using (30).

In a recent publication, [21], Oliveras & Vasan derived a fully nonlinear theory to deduce $\eta(x, t_0)$ from $P(x, -h, t_0)$ in the case of a traveling water-wave without any knowledge of the wave speed. However, the formulation is formidable, and since wave speed is required, operationally, to convert from temporal to spatial data, we do not use the approach of [21].

4. Experimental Apparatus and Procedure

Experiments were conducted in the William G. Pritchard Fluid Mechanics Laboratory in the Department of Mathematics at Pennsylvania State University to create and measure a variety of waves for comparisons of surface reconstructions using the three models (21-23). In these experiments the pressure at the bottom of the fluid and the displacement of the air–water interface were measured simultaneously during wave propagation.

4.1. Apparatus

The wave tank is 50 ft long and 10 inches wide with tempered glass walls and bottom. It was cleaned with alcohol and filled with tap water to a depth greater than the desired depth, h, so that the surface could be cleaned. We cleaned the surface using a fan attached to one side of the tank. It blew a wind that created a surface current that carried contaminants attached to the surface along the length of the tank to the other end (50ft away). There we used a wet vac to vacuum the contaminants along with the top few millimeters of fluid. We used a Lory Type C point gage to measure the resulting water depth h.

We used two types of wave gages: a capacitance gage for measuring surface displacements directly and a pressure transducer mounted into a hole in the bottom glass panel. The pressure transducer was a SEN^{Z}ORS PL6T submersible level transducer with a range of 0-4 in. It provided a 0-5V dc output, which was digitized with an NI PCI-6229 analog-to-digital converter using LabView software. We calibrated this transducer by raising and lowering the water level in the channel. The pressure measurements had a high-frequency noise component, and thus low-pass filters were employed.

We implemented two possible low-pass filters. In the first case, by averaging the Fourier amplitudes of the high-frequency wave numbers we estimated a noise level. All modes with Fourier amplitudes less than or equal to this noise level were set to zero. The noise level was chosen so that the transform $\cosh(kh)$ resulted in a smooth reconstruction. Effectively, this filter picked out the dominant modes. In the second case, the pressure measurements were filtered assuming a suitable cut-off frequency. For instance, data from a measurement of a 1 Hz cnoidal wave was filtered with a cut-off frequency of 10 Hz. This smoothing however does not necessarily regularize the hyperbolic transforms employed in the transfer and heuristic function approach. To do so we replaced the original hyperbolic terms with $\cosh(\alpha kh)$ and $\sinh(\alpha kh)$, where $\alpha = 1$ if $kh < 1$ and $\alpha = 0$

otherwise. Thus when $\alpha = 0$, both transfer and heuristic functions are equivalent to the identity map. In essence, we wish to apply the recovery algorithm only to the shallow water component of the measured signal.

Both low-pass filters produced qualitatively similar results in real space. Further, the frequency corresponding to $kh = 1$ was close to the largest dominant mode picked out by the first method. In the experiments discussed below this was around 2 Hz. The heuristic function, being a nonlinear map from pressure to surface elevation, introduces higher wave number modes into the reconstruction unlike the transfer function approach. The first method of filtering typically retains a small number of dominant modes and so is ideally suited to understanding the nonlinear interactions generated by the heuristic function. However, in practice, we prefer the second method of filtering the pressure measurements since it is physically motivated and relatively simple to implement.

The capacitance-type surface wave gage consisted of a conducting wire coated with the commercially available superhydrophic coating "Rustoleum's NeverWet".The coated wire was connected to two quartz crystals. One had a fixed oscillation frequency and one had a frequency dependent on the water height on the coated wire. The difference frequency was read by a Field Programmable Gate Array (FPGA), NI PCI-7833R. The surface capacitance gage was held in a rack on wheels that was attached to a programmable belt. We calibrated the capacitance gage by traversing the rack at a known speed over a precisely machined, trapezoidally-shaped "speed bump". Time series of surface displacement were obtained using LabView software that controlled the FPGA board.

The output from the pressure and surface gauges consisted of a time series of the pressure and surface displacement at a fixed location respectively. Since the theory for surface reconstruction is based on knowledge of the pressure field, *i.e.*, a spatial measurement, we used the speed of the wave to translate the time series into a spatial measurement. The choice of speed depends on the particular type of wave. Thus for a small amplitude wave that is well approximated by the linearized water-wave equations we chose the phase speed given by the dispersion relation, whereas for more nonlinear waves we used the programmed wave speed. An alternate choice is the shallow water wave speed of $\sqrt{gh}$, where h is the mean depth of the water. We note that all models considered herein require knowledge of wave speed, since all models make a spatial reconstruction out of temporal measurements. The conversion from a temporal measurement to a spatial one involves an assumption on the partial differential equation satisifed by the measured quantity (here

the bottom pressure). In the current work we assume the pressure satisfies an equation of the form

$$p_t + \omega(-i\partial_x)p = 0,$$

where $\omega(k)$ is the dispersion relation. Here we choose either $\omega = ck$ or the expression given by (24). The solution to the above differential equation (assuming periodic boundary conditions) can be written as

$$p(x,t) = \sum_{n\in\mathbb{Z}} e^{in\pi x/L + i\omega(n)t}\mathcal{F}[p_0](n),$$

where p_0 is an initial condition and L is the spatial period of the wave. The conversion from a temporal measurement to a spatial one is equivalent to re-parametrizing the summation above in terms of ω, rather than k. This involves inverting the dispersion relation. Consequently we see the need for a one-to-one relation between ω and k, and we limit the discussion to waves traveling in one direction. Finally we note that the process of temporal to spatial measurment conversion is a type of smoothing in the case of traveling water waves where $k = \omega/c$. Thus choosing a wave speed c, in combination with the $kh = 1$ cutoff, works to bias the reconstruction towards the low frequency modes. Indeed, both transfer and heuristic functions approximate the hydrostatic reconstruction for larger values of c.

The waves were generated with a piston-type paddle made from Teflon and machined to fit the channel with a thin lip around its periphery that served as a wiper with the channel's glass perimeter. This wiper minimized leakage around the paddle during paddle motion. The paddle was attached to a Parker 406 LXR linear motor, controlled using the Aries Controller Program (ACR) 6 software. The motion of this paddle could be precisely programmed to provide a smooth stroke profile with a resolution of 1/42000 inch. The theory for programming the paddle motion is discussed in the next section.

4.2. Theory for wave generation

In order to perform controlled and repeatable experiments, we generated specific known surface profiles. Hence, here we describe a method to translate a given target surface profile $\zeta(x,t)$ into a corresponding motion of the paddle $L(t)$. Assuming the fluid motion is governed by the equations for

inviscid irrotational flow, the velocity potential satisfies the following free-boundary value problem:

$$\phi_{xx} + \phi_{zz} = 0, \qquad (x,z) \in D, \tag{31}$$

$$\phi_t + \frac{1}{2}\left(\phi_x^2 + \phi_z^2\right) + g\eta = 0, \qquad z = \eta(x,t), x > L(t), \tag{32}$$

$$\eta_t + \eta_x \phi_x = \phi_z, \qquad z = \eta(x,t), x > L(t), \tag{33}$$

$$\phi_x = L'(t), \qquad x = L(t), -h < z < \eta, , \tag{34}$$

$$\phi_z = 0, \qquad z = -h, \tag{35}$$

$$\phi_x, \phi_z, \eta \to 0 \qquad \text{as } x \to \infty, \tag{36}$$

where $L(t)$ is the position of the paddle, η is the surface displacement and for convenience we have assumed a semi-infinite wave tank. The fluid domain is given by $D = \{(x,z) : L(t) < x < \infty, -h < z < \eta\}$. The wavemaker problem consists of the following inverse problem: given a surface displacement η consistent with the above boundary-value problem, determine the position of the piston $L(t)$. Typical target profiles ζ are solutions to the water-wave equations (or asymptotically equivalent models for water waves) posed either on the whole line or with periodic boundary conditions. Thus, the target profile is typically not consistent with a vertical impermeable wall at one end of the fluid domain. Consequently, we consider a smooth solution η to (31-36) such that

$$\eta = \begin{cases} f(x,t), & (x,t) \in F, \\ \zeta(x,t), & (x,t) \in Z, \end{cases} \tag{37}$$

where F, Z are such that Z is a region in the (x,t) plane that includes the paddle location $L(t)$ and, for every fixed t, is bounded above in x. Further we take $F \cup Z = \{(x,t) : t > 0, L(t) < x < \infty\}$, see Figure 4.

Our approach to the wavemaker problem follows the theory presented in [25], which uses conservation of mass to obtain an ordinary differential equation for L. In that model, conservation of mass amounts to a balance of the normal flux at $x = 0$, due to the paddle motion, and the normal flux at the surface, since the normal velocities at the bottom boundary and at $x \to \infty$ are zero. This balance is a necessary condition for any solution to (31-36). That is,

$$\int_{\partial D} \frac{\partial \phi}{\partial n} = 0,$$

where $\partial/\partial n$ denotes the normal derivative in the outward normal direction. Thus, as a consequence

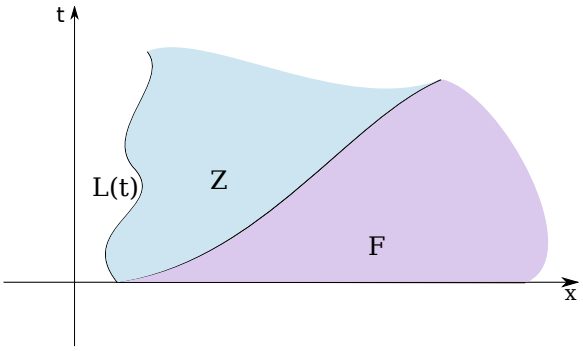

Figure 4

of (33-36), we have

$$-L'(t)[\eta(L(t),t)+h]+\int_{L(t)}^{\infty}\eta_t\,dx=0,$$
$$\Rightarrow \frac{dL}{dt}=\frac{1}{\eta(L(t),t)+h}\int_{L(t)}^{\infty}\eta_t\,dx. \tag{38}$$

Equation (38) forms the basis for the wavemaker problem. For a given profile η, we solve the above ordinary differential equation for $L(t)$. In the following, we derive the associated forcing equation for certain classes of target profiles.

1. **Periodic traveling waves**: Here we take

$$\eta=\begin{cases} f(x-ct), & x-ct\geq\xi_0,\\ \zeta(x-ct), & x-ct<\xi_0,\end{cases},$$

where $\zeta(\xi)$ is a target profile, $f(\xi)$ is a traveling front that vanishes as $\xi\to\infty$ and $\xi_0>L(t)$ for all t. Once again $\eta_t=-c\eta_\xi$ and (38) gives

$$\frac{dL}{dt}=\frac{c\,\zeta(L-ct)}{\zeta(L-ct)+h}.$$

The periodic waves generated here are KdV cnoidal waves (particular periodic solutions of the Korteweg de Vries equation), such that (see [26])

$$\zeta(\xi)=t_0+a_0\mathrm{cn}^2\left(\frac{2K(m)\xi}{\lambda},m\right), \tag{39}$$

where a_0 is the trough-to-crest height of the wave, m is the elliptic modulus [27, 28], $K(m)$ is the complete elliptic integral of the first kind [27, 28], t_0 is the trough level and λ is the

wavelength. Given a_0, the frequency f_0 and mean depth of fluid h, one obtains the remaining quantities from the following relationships:

$$
\begin{aligned}
t_0 &= \frac{a_0}{h}\left(1 - m - \frac{E(m)}{K(m)}\right), \\
\lambda &= h\sqrt{\frac{16}{3}\frac{mh}{a_0}}K(m), \\
c &= \sqrt{gh}\left[1 + \frac{a_0}{mh}\left(1 - \frac{m}{2} - \frac{3E(m)}{2K(m)}\right)\right], \\
c &= \lambda f_0,
\end{aligned}
$$

where $E(m)$ is the complete elliptic integral of the second kind [27, 28], c is the speed of the wave and g is the acceleration due to gravity. Combining the last three equations above, one obtains the elliptic modulus using a simple Newton's method.

2. **Reflected waves**: Reflected cnoidal waves were generated when the cnoidal wave train generated as above reached the end of the wave tank. Measurement stations for surface height and bottom pressure were the same in the case of a single traveling wave. The reflected wave was noted to be traveling at the same speed as the original wave however in the opposite direction.

3. **Wave group**: A wave packet is produced by considering a target profile of the form $\zeta = \zeta_1 + \zeta_2$ where $\zeta_i = A\sin(k_i x - w_i t)$. Here $|w_1 - w_2|$ is small and k_i is obtained by solving the linear dispersion relation $w_i^2 = gk_i \tanh(k_i h)$. Of course, the amplitude should be small enough such that the linear approximation is valid. Under these assumptions, the differential equation for $L(t)$ has a similar form as in the previous cases, the numerator on the right-hand side being $c_1\zeta_1 + c_2\zeta_2$ with $c_i = w_i/k_i$.

5. Results

We use measurements of time series of pressure measured at a point at the bottom of the wavetank to reconstruct the corresponding time series of the surface displacement. We compare the reconstruction with direct measurements of the surface displacement. The theory assumes that the wave fields are traveling waves. In previous work we showed comparisons for solitary wave forms modeled by KdV solitons [1]. Here we look at the periodic case by generating KdV cnoidal waves. In order to see how the theory works for more realistic shallow-water conditions, we also

look at wave systems outside the range of validity of the theory, including reflected cnoidal waves, and wave groups. In the comparisons below we define the transfer function approach to be the one obtained from linear water-wave theory. This is equivalent to (22), which is (1) with the empirical constant $N = 1$.

5.1. Cnoidal wave

To look at the reconstruction for periodic waves, we generated a cnoidal wave, (39) using a frequency of $f_0 = 1$ Hz and crest-to-trough height of $a_0 = 1.9$ cm in water with quiescent depth $h = 6.16$ cm as discussed in §4. The speed of the cnoidal wave profile was within 0.5% of the shallow water speed $\sqrt{gh}$, where g is the acceleration due to gravity. We note that because of dissipation the measured wave amplitudes do not agree with the amplitude programmed at the wavemaker.

Figure 5 shows results. The measured time series is shown in Figures 5A–5C along with reconstructions using the hydrostatic approximation (21), the transfer function (22) that accounts for linear wave motion, and the heuristic model (23) obtained from the fully nonlinear model in [1]. We note that in the troughs, the measured time series has a bump that is not captured by the hydrostatic or transfer functions, and only slightly captured by the heuristic model. The source of this bump in the experiments is the contact line between the cnoidal wave crest and the glass sidewalls. The interaction there results in a short-crested wave at symmetric angles from both sidewalls. They intersect in the trough of the cnoidal wave and look like an inverse Kelvin wake.

Overall, we see that in this experiment, the hydrostatic approximation is the least accurate, while the transfer and heuristic models agree reasonably well with the measurements; the heuristic model is more accurate than the transfer function in capturing the peak amplitude. Another test of the models is to look at their Fourier amplitudes. Figure 5D shows the ratio of predicted to measured Fourier amplitude, with predictions from the transfer and heuristic models. An amplitude ratio of 1 corresponds to agreement between measurements and model predictions. In the reconstructions, one must pick a wavenumber cut-off for the Fourier transforms because of the factor of $\cosh(kh)$ that appears in the transfer function and the heuristic formula. This cut-off is clear in the ratio of Fourier amplitudes for the transfer function (shown by the gray, dashed curve in Figure 5D) and occurs at about 2.5 Hz. However, the nonlinearity in the heuristic formula (shown by the black, dashed curve in Figure 5D) allows for nonlinear interactions among Fourier modes, so that it fills in the spectrum regardless of the cut-off.

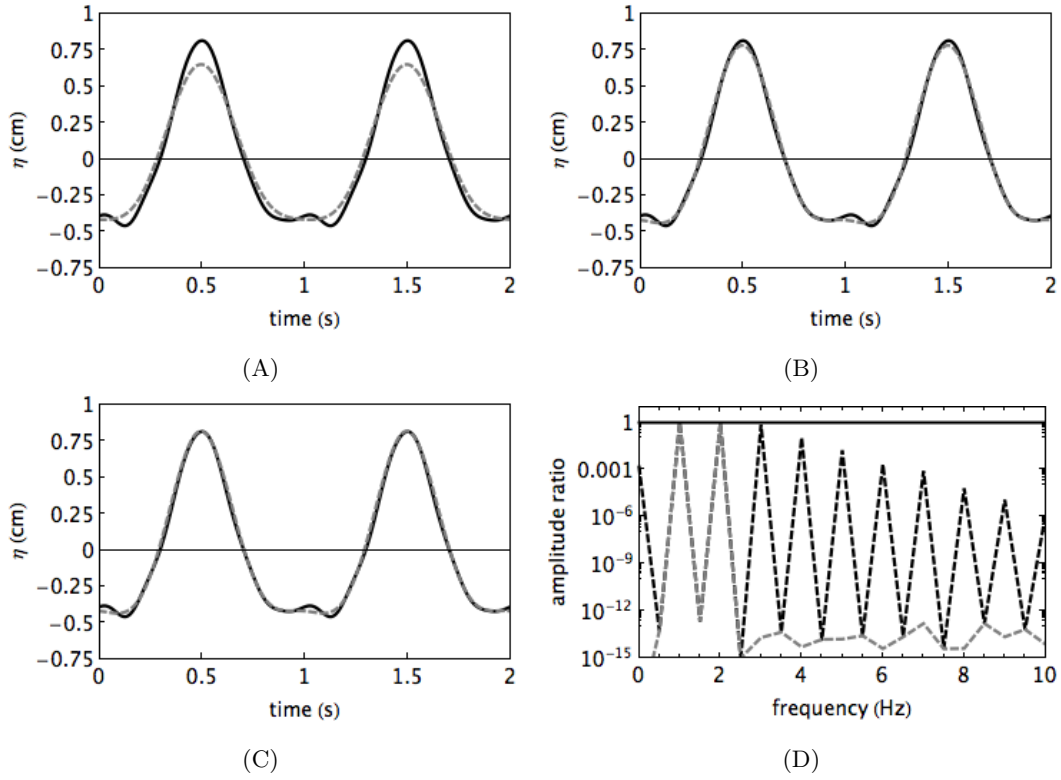

Figure 5: Reconstruction of cnoidal waves. (A-C) Time series of measured and reconstructed surface displacements. Measurements are shown by the solid black curve. The dashed, gray curve represents: (A) the hydrostatic approximation, (21); (B) the transfer function, (22); (C) the heuristic formula, (23); (D) The ratio of the Fourier amplitudes of the reconstructed elevation to the measured elevation for the transfer function (dashed, gray curve) and heuristic formula (dashed, black curve). The solid black line shows the spectral goal of a successful reconstruction.

5.2. Reflected cnoidal waves

In the field, waves are reflected by beaches, other topographic features and man-made fixtures. To see if the theory presented here, which assumes traveling waves (necessarily in one direction) works in this regime, even though it is outside the range of validity of the theory, we did experiments using cnoidal waves that were generated at one end of the tank, as described in §4.2 and allowed to reflect off the wall at the other end of the tank. Below we present results for a cnoidal wave generated with $f_0 = 1$ Hz, $a_0 = 1.9$ cm and $h = 6.16$ cm.

Figure 6 shows results. The measured time series is shown in Figure 6A–6C along with reconstructions using the hydrostatic approximation (21), the transfer function (22) that accounts for linear wave motion, and the heuristic model (23) obtained from the fully nonlinear model in [1].

Overall, we see that in this experiment, the hydrostatic approximation is the least accurate. The transfer and heuristic models are in reasonable agreement with the measurements of the surface displacements, with the heuristic formula performing best overall. As discussed in §5.1, the Fourier amplitudes provide further information. Figure 6D shows the ratio of predicted to measured Fourier amplitude, with predictions from the transfer and heuristic models. Again, the wavenumber cut-off for the Fourier transforms due to the factor of $\cosh(kh)$ that appears in the transfer function and the heuristic formula occurs at about 8 Hz. Thus, the reconstruction using the transfer function has negligible energy in frequencies above this cut-off, while the heuristic formula, due to its allowance for nonlinear interactions, has energy in the higher frequency modes, as does the spectrum from the measurements.

5.3. Wave groups

When swell approaches shallow water from deep water, it typically arrives in wave groups. Again, wave groups are outside the range of validity of the present theory, which assumes that all waves travel at a single speed. However, we did comparisons with wave groups, which were generated as discussed in §4.2. Here we used $A = 0.5$in, $\omega_1 = 2\pi$ s^{-1}, and $\omega_2 = 0.1 \cdot 2\pi$ s^{-1}. The results are shown in Figure 7.

All of the three models considered get the phasing of the individual waves correct. Again, the hydrostatic approximation underestimates the wave amplitudes, while the transfer and heuristic models are in reasonable agreement with the measurements of the surface displacements. The heuristic formula performs best overall. As before, the spectrum shows that the nonlinear coupling

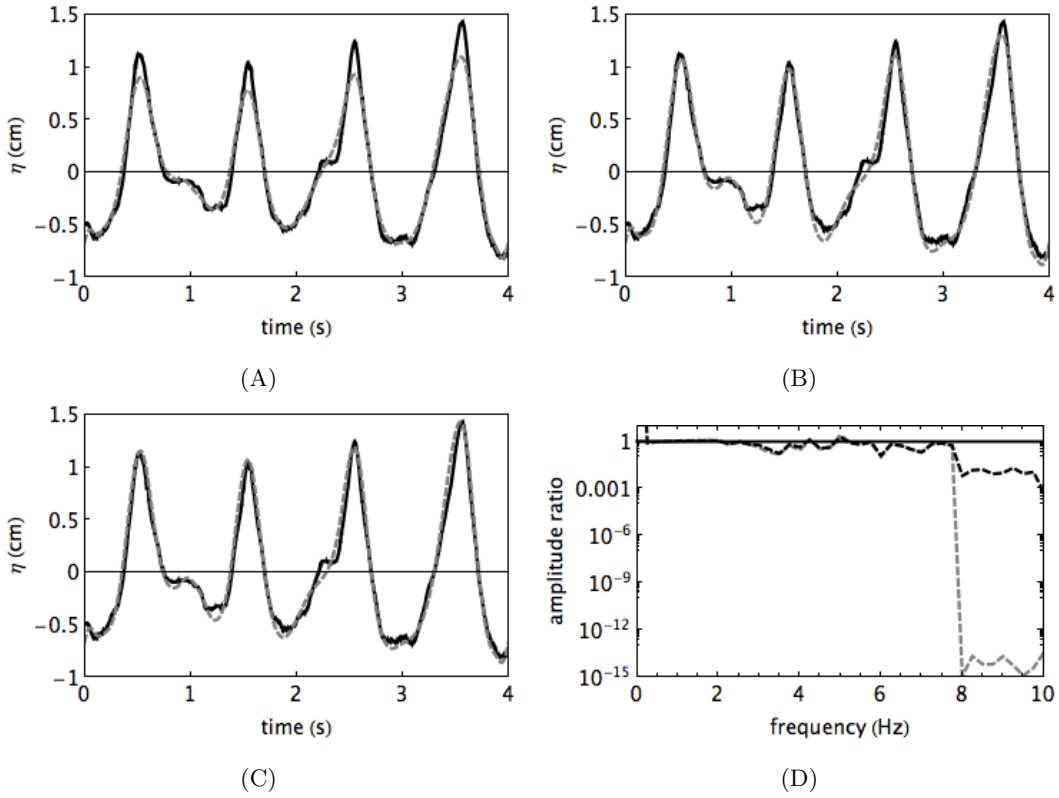

Figure 6: Reconstruction of reflected cnoidal waves. (A-C) Time series of measured and reconstructed surface displacements. Measurements are shown by the solid black curve. The dashed, gray curve represents: (A) the hydrostatic approximation, (21); (B) the transfer function, (22); (C) the heuristic formula, (23); (D) The ratio of the Fourier amplitudes of the reconstructed elevation to the measured elevation for the transfer function (dashed, gray curve) and heuristic formula (dashed, black curve). The solid black line shows the spectral goal of a successful reconstruction.

of modes allowed in the heuristic formula generates energy at modes above the cut-off for analysis; so the energy spectrum obtained from the heuristic formula is much closer to that of the measured spectrum than is that of the transfer function.

6. Summary

We have proposed alternative formulae to the standard hydrostatic approximation and transfer function for reconstructing a wave surface that is measured using a pressure transducer. These formulae are approximations and extensions to the fully nonlinear, non-local formulae derived by [1] that assumes traveling waves.The proposed formulae allow the pressure transducer to be at any depth in the water column and can account for a uniform vorticity.

If the transducer is at the bottom of the water column, then one can approximate the water surface displacement using the heuristic formula

$$\eta = \frac{\mathcal{F}^{-1}\left[\cosh(kh)\mathcal{F}\left[\frac{p}{g}\right]\right]}{1-\mathcal{F}^{-1}\left[k\sinh(kh)\mathcal{F}\left[\frac{p}{g}\right]\right]},$$

which is (23). If the pressure transducer is at a depth of $|z_0|$ from the still water surface, then one first uses the pressure measurements at this depth to find the pressure at the bottom using

$$\mathcal{F}[p] = \operatorname{sech}(k(h-z_0))\mathcal{F}[p_0],$$

which is (30). Then one applies the heuristic formula above given by (23). Further we extended the fully nonlinear formulation to allow for a uniform vorticity in (A.1).

In a previous paper [1], we tested the fully nonlinear theory and various approximations with measurements of solitons and found that, other than the fully nonlinear model, the heuristic formula gave the best agreement with measurements. Here we compared reconstructions using the hydrostatic approximation (21), the transfer function (22) and the heuristic formula (23) with measurements of (periodic) cnoidal waves and with two wave systems that are outside the range of validity of the theory: reflected cnoidal waves and wave groups. We found that since the heuristic formula includes nonlinearity, its amplitude spectrum more closely approximates that of the surface data. The hydrostatic approximation is inadequate in reconstructing the measured time series, while both the transfer and heuristic formulae reproduce it reasonably well. Nevertheless,

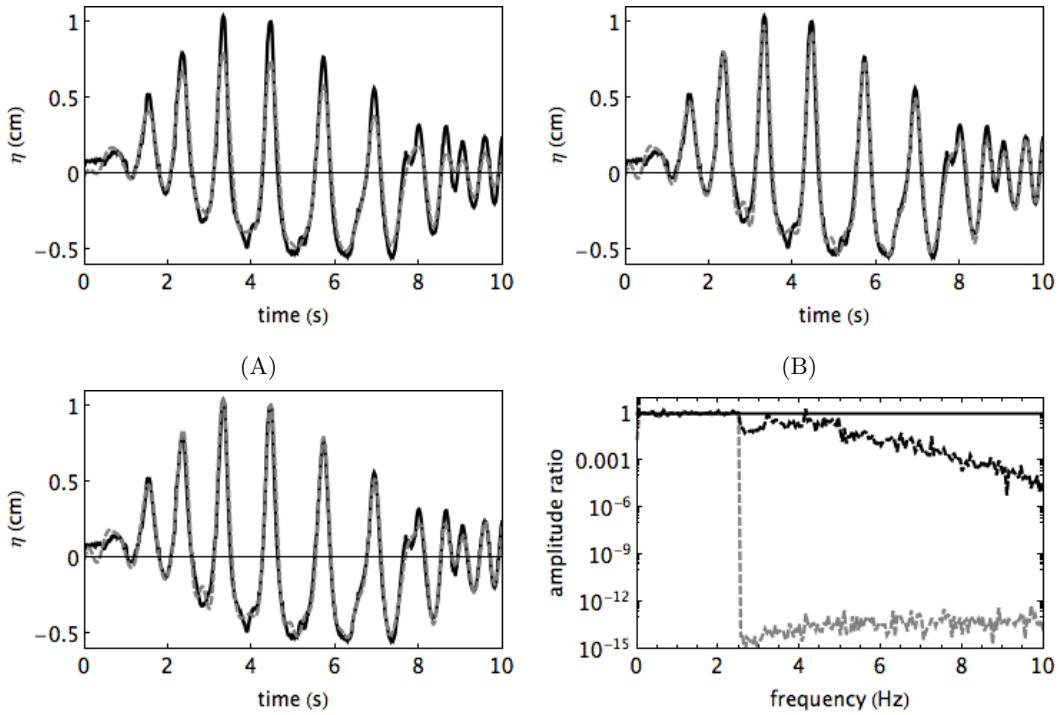

Figure 7: Reconstruction of a wave group. (A-C) Time series of measured and reconstructed surface displacements. Measurements are shown by the solid black curve. The dashed, gray curve represents: (A) the hydrostatic approximation, (21); (B) the transfer function, (22); (C) the heuristic formula, (23); (D) The ratio of the Fourier amplitudes of the reconstructed elevation to the measured elevation for the transfer function (dashed, gray curve) and heuristic formula (dashed, black curve). The solid black line shows the spectral goal of a successful reconstruction.

in a comparison of the heuristic and transfer functions, we note that the heuristic formula gives results that are about 5% more accurate and the spectrum of the heuristic formula more accurately describes that of the data. The heuristic formula is straightforward to use, requiring just one more Fourier transform than the transfer function. Further the assumption of traveling waves, which is inherent in both the heuristic formula and transfer function, does not seem to be a limiting factor in accuracy. Thus, we conclude that the heuristic formula provides a better inverse map of pressure measurements to surface displacement than does the transfer function.

Acknowledgments

BD and VV acknowledge support from the National Science Foundation under grant NSF-DMS-1008001. DH acknowledges support from the National Science Foundation under grants NSF-DMS-0708352 and NSF-DMS-1107379. KO gratefully acknowledges support from the National Science Foundation under grant DMS-1313049 and AMS-Simons Travel Grant. We thank Robert Geist for construction of the laboratory apparati and Rod Kreuger for building the FPGA wave gage system. Any opinions, findings, and conclusions or recommendations expressed in this material are those of the authors and do not necessarily reflect the views of the funding sources.

Appendix A. Reconstruction in the presence of vorticity

The basic surface reconstruction algorithm extends to the case of a two-dimensional traveling water wave in the presence of constant vorticity. The case of a constant vorticity represents the simplest possible situation of a wave-current interaction [29–34] and exhibits new and interesting physical phenomena. As a result of wave-current interaction, flows develop stagnation points (where the fluid velocity is equal to the velocity of the wave) in the interior of the fluid domain. Further, there exist regions of the fluid where the pressure is below the atmospheric value [20, 35]. Additionally, when stagnation points are present in the fluid, the maximum pressure at the bottom boundary is no longer beneath the crest of the wave, *i.e.*, there is a phase shift between the maximum of the bottom pressure and the wave crest, see [20]. All these phenomena appear even when considering constant vorticity.

In this section, we summarize the results of [20] relevant to the surface reconstruction algorithm. For the case of solitary waves with generic vorticity, see [36]. In the following presentation, we

restrict to two-dimensional inviscid traveling water waves with speed c and constant vorticity γ. The fluid motion may be described using a stream-function formulation given by

$$\begin{aligned} \Delta\psi &= -\gamma, && -h < z < \eta(x), \\ \psi_x &= 0, && \text{at } z = -h, \\ \frac{\psi_x^2}{2} + \frac{(\psi_z - c)^2}{2} + gz - c\gamma z + \gamma\psi &= \frac{c^2}{2}, && \text{at } z = \eta, \\ (\psi_z - c)\eta_x + \psi_x &= 0, && \text{at } z = \eta. \end{aligned}$$

As in the previous section, the horizontal boundary conditions are assumed to be either periodic or vanishing at infinity. We normalize the stream function ψ so that $\psi - cz = 0$ at $z = \eta$. Consequently, $\psi(x, -h) = -m$ where m is the mass flow rate which we assume is a known constant. Let σ_s be the sign of the horizontal fluid velocity at the free surface. We take $\sigma_s = 1$ to indicate a flow in the positive $x-$direction in a frame relative to the wave and $\sigma_s = -1$ to indicate the flow in the negative direction. Similarly, σ_b represents the direction of the fluid flow at the bottom boundary $z = -h$. Finally, as in the irrotational case, the Bernoulli condition is valid in the bulk of the fluid domain. As before, this permits one to translate the pressure measured at the bottom boundary into a condition on the horizontal fluid velocity [20].

Let φ be the irrotational fluid stream function defined by $\psi = \varphi - \gamma z^2/2 + (c + \sigma_s|c|)z$. Thus φ is a harmonic function in the fluid domain. Further, as a consequence of the bulk Bernoulli condition we have

$$\varphi_z(x, -h) = \sigma_b \left(-|\gamma h + c| + \sqrt{(\gamma h + c)^2 - 2p} \right),$$

where p is the non-static component of the bottom pressure $P(x, -h)$, *i.e.*,

$$p = P(x, -h)/\rho - gh - \gamma m + \gamma^2 h^2/2 + c\gamma h.$$

As seen from the above expression, we require m, σ_s, σ_b, γ and c to define the non-static pressure and the fluid velocity at the bottom boundary. Having defined these quantities, the analysis follows that used to obtain (19). We simply state the associated nonlinear nonlocal expression for the surface profile.

$$\sigma_s \left(-|c| + \sqrt{\frac{c^2 - 2g\eta}{1 + \eta_x^2}} \right) = \frac{\sigma_b}{2\pi} \int_{-\infty}^{\infty} e^{ikx} \cosh(k(\eta + h)) \mathcal{F}\left\{ -|\gamma h + c| + \sqrt{(\gamma h + c)^2 - 2p} \right\}(k) dk. \tag{A.1}$$

We note that, for nontrivial flows with $\gamma = 0$, no stagnation points exist within the fluid and thus $\sigma_s = \sigma_b$. Consequently, (A.1) reduces to (19) in this case.

[1] K. Oliveras, V. Vasan, B. Deconinck, D. Henderson, Recovering the water-wave profile from pressure measurements, SIAM J. Appl. Math. 72 (2012) 897–918.

[2] G. Stokes, Mathematical and Physical Papers, Vol. 1, Johnson Reprint Corp. NY & London, 1966.

[3] U. A. E. W. E. Station, Shore Protection Manual, Vol. 1m 4th ed, Vicksburg Miss MI, 1984.

[4] C. T. Bishop, M. A. Donelan, Measuring waves with pressure transducers, Coastal Engineering 11 (1987) 309–328.

[5] D. Y. Lee, H. Wang, Measurement of surface waves from subsurface guage, 1984.

[6] A. O. Bergan, A. Torum, A. Traetteberg, Wave measurements by pressure type wave gauge, Proc. 11th Coastal Eng. Cong. ASCE (1968) 19–29.

[7] C.-H. Tsai, M.-C. Huang, F.-J. Young, Y.-C. Lin, H.-W. Li, On the recovery of surface wave by pressure transfer function, Ocean Engineering 32 (2005) 1247–1259.

[8] J.-Y. Chen, Three dimensional nonlinear pressure transfer function, Coastal Engineering 11111 (2000) 3111109–3111128.

[9] Y. Y. Kuo, Y. F. Chiu, Transfer function between the wave height and wave pressure for progressive waves, Coastal Engineering 23 (1994) 81–93.

[10] A. Baquerizo, M. A. Losada, Transfer function between wave height and wave pressure for progressive waves, by Y.-Y. Kuo and J.-F. Chiu: comments, Coastal Engineering 24 (1995) 351–353.

[11] Y. Y. Kuo, Y. F. Chiu, Transfer function between the wave height and wave pressure for progressive waves: reply to the comments of a. baquerizo and m. a. losada, Coastal Engineering 24 (1995) 355–356.

[12] D. Clamond, A. Constantin, Recovery of steady periodic wave profiles from pressure measurements at the bed, J. Fluid Mech. 714 (2013) 463–475.

[13] A. Constantin, On the recovery of solitary wave profiles from pressure measurements, J. Fluid Mech. 699 (2012) 1–9.

[14] H.-C. Hsu, Recovering surface profiles of solitary waves on a uniform stream from pressure measurements, DCDS-A 34 (2014) 3035–3043.

[15] D. Clamond, New exact relations for easy recovery of steady wave profiles from bottom pressure measurements, J. Fluid Mech. 726 (2013) 547–558.

[16] J.-C. Tsai, C.-H. Tsai, H.-M. Tseng, Pressure derived wave height using artificial neural networks, Proc Oceans'08 MTS/IEEE Kobe-Techno-Ocean (2008) 1–8.

[17] J.-C. Tsai, C.-H. Tsai, Wave measurements by pressure transducers using artificial neural networks, Ocean Engineering 36 (2009) 1149–1157.

[18] A. B. Kennedy, R. Gravois, B. Zachry, R. Luettich, T. Whipple, R. Weaver, J. Reynolds-Fleming, Q. J. Chen, R. Avissar, Rapidly installed temporary gauging for hurrican waves and surge, and application to hurricane gustav, Continental Shelf Research 30 (2010) 1743–1752.

[19] M. J. Ablowitz, A. S. Fokas, Z. H. Musslimani, On a new non-local formulation of water waves, J. Fluid Mech. 562 (2006) 313–343.

[20] V. Vasan, K. L. Oliveras, Pressure beneath a traveling wave with constant vorticity, Disc. & Cont. Dyn. Sys. Ser. 34 (2014) 3219–3239.

[21] K. L. Oliveras, V. Vasan, Relationships between the pressure and the free surface independent of the wave speed, Contemporary Mathematics 635 (2015) 157–173.

[22] B. Deconinck, K. L. Oliveras, V. Vasan, Relating the bottom pressure and the surface elevation in the water wave problem, J. Nonlinear Math. Phys. 19 (suppl. 1) (2012) 1240014, 11.

[23] A. Constantin, W. Strauss, Pressure and trajectories beneath a Stokes wave, Communications on Pure and Applied Mathematics 63 (2010) 533–557.

[24] B. Deconinck, K. Oliveras, The instability of periodic surface gravity waves, J. Fluid Mech. 675 (2011) 141–167.

[25] D. G. Goring, F. Raichlen, The generation of long waves in the laboratory, Proc. 17th Intl. Conf. Coastal Engrs., Sydney, Australia 11111 (1980) 3111109–3111128.

[26] M. W. Dingemans, Water Wave Propagation Over Uneven Bottoms, World Scientific, 1997.

[27] NIST Digital Library of Mathematical Functions, http://dlmf.nist.gov/, Release 1.0.9 of 2014-08-29, online companion to [28].
URL http://dlmf.nist.gov/

[28] F. W. J. Olver, D. W. Lozier, R. F. Boisvert, C. W. Clark (Eds.), NIST Handbook of Mathematical Functions, Cambridge University Press, New York, NY, 2010, print companion to [27].

[29] A. Constantin, W. Strauss, Exact steady periodic water waves with vorticity, Communications on Pure and Applied Mathematics 57 (2004) 0481–0527.

[30] A. Constantin, W. Strauss, Rotational steady water waves near stagnation, Phil. Trans. R. Soc. A. 356 (2007) 2227–2239.

[31] E. Wahlen, Steady periodic capillary waves with vorticity, Ark. Mat. 44 (2006) 367–387.

[32] E. Wahlen, Steady water waves with a critical layer, J. Diff. Eq. 246 (2009) 2468–2483.

[33] J. Ko, W. Strauss, Effect of vorticity on steady water waves, J. Fluid Mech. 608 (2008) 197–216.

[34] J. Ko, W. Strauss, Large-amplitude steady rotational water waves, Eur. J. Mech. B/Fluids 27 (2) (2008) 96–109.

[35] A. T. D. Silva, D. H. Peregrine, Steep, steady surface waves on water of finite depth with constant vorticity., J. Fluid Mech. 195 (1988) 281–302.

[36] D. Henry, On the pressure transfer function for solitary water waves with vorticity, Math. Ann. (2013) 1–8.